

N92-27802

PRESENT STATUS OF THE MIT/NASA LANGLEY 6-INCH MSBS

Timothy Schott, Thomas Jordan, and Taumi Daniels
Langley Research Center

Charles Alcorn
Old Dominion University

PRECEDING PAGE BLANK NOT FILMED

ABSTRACT

The paper describes the latest improvements made to the MIT/NASA Langley 6 Inch Magnetic Suspension and Balance System and its present operational capabilities. Since its relocation from MIT in 1984, the system has suffered from reliability problems with original equipment. System performance is ultimately limited by noise and antiquated power supplies. Although a limited amount of funding and man hours has been expended, some significant improvements have been made to the system. The design and implementation of a new electro-magnetic position sensor has significantly reduced system noise and drift.

In January 1991, the system was demonstrated fully operational for the first time since its arrival at NASA Langley Research Center. An ogive cylinder test model was suspended while running the wind tunnel at its maximum of approximately Mach 0.5. Since that time, other aerodynamic models have been suspended with wind on.

In addition, the simulation of low-speed cavity store separation using an ogive cylinder test model is described. Methods used for flow visualization for this test are also discussed. The system is ideally suited for this type of low speed testing.

INTRODUCTION

The 6 Inch Magnetic Suspension and Balance System (MSBS) was originally designed and constructed from 1966 to 1969 under contract for NASA Langley Research Center (LaRC) by Massachusetts Institute of Technology (MIT), and was used there for research until 1982. The 6 Inch MSBS was then relocated to NASA LaRC and installed in 1984. For a period of five years, work on the system was limited to minor system improvements and maintenance. The system has suffered from reliability problems with the original equipment. As a result, significant down time has been experienced. In addition, electrical noise in the feedback control loops and antiquated power systems limit system performance.

In September 1989, an initiative to make the 6 Inch MSBS fully operational began.

Although a limited amount of funding and man hours has been expended, some significant improvements have been made to the system. Among the improvements made to the system are new electro-magnetic position sensor (EPS) electronics, control system rewiring, and new water-cooled resistors. The 6 Inch MSBS is unique among wind tunnels of this type due to its model position measurement system. All other magnetic suspension wind tunnels use optical methods.

In January 1991, an ogive cylinder test model was suspended at a Mach number of 0.5, demonstrating the system's fully operational status. The system reliability and performance before this time prevented any wind-on testing. Since then, other aerodynamic models have been suspended at lower mach numbers.

In addition, the simulation of low-speed cavity store separation using an ogive cylinder model was performed. Due to the absence of mechanical supports for the model, which are necessary for conventional wind tunnel models, an interference-free simulation resulted. As a result, the system is uniquely suited for this type of low speed testing. Flow visualization using vaporized propylene glycol further enhanced the store separation.

SYSTEM DESCRIPTION

The basic components comprising the 6 Inch MSBS are the subsonic wind tunnel, magnetic assembly, control electronics, and the power supply system. Each of these components is briefly described below.

A more detailed description of the system may be found in reference 1.

Subsonic Wind Tunnel

A subsonic, open circuit wind tunnel was fabricated by MIT for use with the magnetic balance. Figures 1 and 2 are views of the wind tunnel looking downstream and upstream, respectively. The contraction, which slides away from the test section for access, was constructed of molded plywood. Two settling chambers and a honeycomb, fabricated using ordinary drink straws, are located upstream of the contraction to reduce flow nonuniformities. The octagonal test section, which is located within the magnetic assembly, is transparent acrylic with an inside dimension of 6.25 inches and a length of 36 inches. A slight taper is employed to account for boundary layer growth. A two-piece mahogany diffuser with access doors is located between the magnetic assembly and the squirrel cage fan. The soft wood inflicts minimal damage to a test model if control is lost with wind on. The wind tunnel is capable of operating at a Mach number of 0.6.

Magnetic Assembly

A symmetrical group of subassemblies with a variety of separate control coils produce the required magnetic fields for model positioning within the test section. Figure

3 shows end and sectional views of the magnet configuration.

Two circular solenoid coils located fore and aft of the center provide both a uniform magnetizing, or bias field, as well as an axial gradient field. Each coil assembly is multiwound with separate electrical connections allowing a Helmholtz pair to be driven separately from axial control coils.

The ends of the magnetic assembly are made of two octagonal silicon steel cores with four poles, each angled toward the center of the assembly. The control windings for lift and side positioning are located between the poles and each set of four are wired in series. Current flowing through a coil excites the two adjacent poles. Therefore, the lift coils are located on each side of the core inducing a vertical flux path as seen in the figure.

The fields controlling pitch and yaw are produced by two pairs of "saddle coils" located internally between the axial solenoids and the test section. MIT chose a complicated arrangement over a simpler design to improve the field homogeneity. An inner pair of coils are rolled at 45 degrees from the vertical and an outer pair are oriented 90 degrees to the inner pair. The primary disadvantage of this arrangement is the limited visual access to the test section. An alternate configuration would have been four identical coils fitting together to form a single cylinder. The chosen configuration relies on vector addition of the field components produced at 45 degrees to the Y and Z axes. An electronic crossover circuit is necessary to mix the pitch and yaw position signals to compensate for the inherent 45 degree fields. MIT also experimented with mixing the current feedback signals for alignment purposes and improved stability. The pitch and yaw system works well for static demonstrations, but has been avoided for high speed flow testing due to difficulties with damping high frequency oscillations.

Control Electronics

The feedback control loop of the MSBS primarily consists of an electromagnetic position sensor (EPS), and compensation electronics.

Electromagnetic Position Sensor

The 6 Inch MSBS is the only magnetic suspension system that does not measure model position optically. Instead, it utilizes the linear variable differential transformer concept, resulting in superior range of model position measurement. The EPS consists of a multi-coil sensor, power amplifier, and demodulation electronics, and can measure aerodynamic model position in five degrees of freedom. The original design is presented in reference 1, and a brief explanation of EPS operation follows.

The EPS coils are configured as a multicoil differential transformer whose primary windings, a Helmholtz pair, are excited by a 20 kHz carrier sinewave. Seven pairs of symmetric, electrically opposed secondary coils are positioned to sense one axial, three vertical, and three horizontal position components. In the absence of an aerodynamic

model, voltages induced in each secondary coil pair mostly cancel due to their geometric symmetry. The presence of a ferromagnetic or electrically conductive model distorts magnetic coupling between primary and secondary windings so that amplitudes of differential voltages appearing between coil pairs are dependent upon model position. Analog circuitry adds or subtracts appropriate components to provide measurements of axial, vertical, and horizontal positions, as well as pitch and yaw angles. In particular, the three vertical components are combined to sense pitch angle and vertical position. Similarly, the three horizontal components are combined to sense yaw angle and side position.

The EPS electronics were redesigned and a complete description of the original and upgraded circuitry can be found in reference 2. The major difference in the new signal processing scheme is in the order of operations. The new design demodulates each bandpass filtered differential coil voltage with its own reference before mixing with other demodulated signals. The old design incorporates extra filtering stages and mixes the differential coil voltages prior to demodulation. Only one reference signal was used for demodulation, resulting in reduced signal amplitude due to phase differences between signals. Thus, this source of position measurement error is corrected in the new design.

After initially reporting on the redesigned EPS, the actual hardware was tested and installed within the system. Only a few minor modifications to the hardware were required. The implemented circuit has a modular design such that the following subcircuits reside on separate printed circuit boards: primary and nulling reference voltage generator board, axial coil and axial position board, vertical coil 1 and lift board, vertical coil 2 and pitch board, vertical coil 3 board, horizontal coil 1 and side board, horizontal coil 2 and yaw board, and horizontal coil 3 board. The printed circuit boards were designed to be interchangeable with only slight modification, and each fits into a particular slot in the EPS electronics chassis backplane. For example, a blank printed circuit board could be populated, and appropriate jumpers would modify the board for a particular slot in the backplane. The backplane is wired to provide power and inter-board signal paths.

As a result of the new design changes, performance has improved. One aspect of performance has been characterized by reduced drift. Figure 4 is a plot of the drift of all five channels of DC position voltage versus time. For each channel of data, the initial data value is subtracted from subsequent values. The drag position measurement has a full scale value of ± 12.5 V dc. The worst case drift is less than 0.1 % of FS/ hr. This performance is a considerable improvement over the older design, and is mainly due to the integrated circuit technology and the new signal processing scheme.

Compensation System

With the exception of replacement operational amplifiers and minor modifications, the original compensation electronics are still in use. The basic blocks are an input summing stage in which a DC offset may be added for model position changes, an integrator stage, and three lead-lag stages in series.

A mixer is used for combining proportional, integral, and compensated signals. A current feedback signal is mixed with the compensated control signal in the final stage for improved model stability. Except for pitch and yaw crossover circuits, the circuitry for each of the five degrees of freedom is basically identical. Sliding modular circuit cards are used for access to various gain potentiometers and lead-lag component switching.

This design reduces noise by eliminating long wires from panel switches to filter components. Originally, all interconnections within the compensation system were made through a patch panel for experimental purposes. The system was unreliable due to corroded contacts and is presently hard-wired.

Power Supply System

Many of the reliability problems and performance limitations of the 6 Inch MSBS are directly related to the power supply system. While at Langley, more man-hours were consumed repairing and modifying power equipment than were expended to improve system performance. MIT modified the power supply system configuration several times to increase drive current capability. The present scheme is an effective system using custom designed and salvaged components. Figure 5 is a basic schematic of the existing power supply subsystems.

The primary supplies for controlling the translational degrees of freedom are uniquely designed full wave rectifiers utilizing thyatron tubes for switching three-phase 440 Vac. Since the thyatron supplies are unipolar, they are oppositely biased through water cooled resistors by a regulated d-c power supply.

The load current may be varied in magnitude and polarity by controlling the current output of the thyatron units. A 250 V, 100 A unit is used for lift, while 120 V, 50 A units are used for side and drag. The thyatron supplies are driven directly by the ± 15 V control signals.

The regulated d-c supply consists of two B-47 aircraft starters. The two stacked units each contain two power supplies which rectify three phase 440 Vac into regulated 28 Vdc up to 1000 amperes. The four power supplies are wired in series and tapped at different points to provide appropriate voltage levels to each subsystem. The drag control coils are provided with 112 V, while lift and side are each supplied with 28 V. In addition, the Helmholtz pair for the uniform magnetizing field is driven by the 56 V tap. Before the procurement of the aircraft starters, one MIT configuration included d-c welders.

Though the saddle coils for pitch and yaw were originally driven by thyatron supplies, a motor-generator set has been in use in recent years. A large a-c motor drives three 1943 vintage aircraft generators to their maximum rpm range. The generators produce a maximum of 30 Vdc at several hundred amperes. The generators were modified by MIT to allow their fields to be driven by bi-polar, solid-state servo amplifiers

producing ± 40 Vdc at 15 A. This design allows high current of either polarity, avoiding the need for a separate bias supply. The inner saddle coils are driven by a single generator while the outer saddle coils are driven by two generators in series. MIT intended to use a similar system for all degrees of freedom as an alternative to expensive bi-polar switching power supplies.

Water-Cooled Resistors

The present configuration of the power supplies and positioning electromagnets requires power resistors to properly bias the coil loads. These low valued resistors have the potential to generate large amounts of heat, and need to be cooled. The original system used individually crafted water-cooled power resistors as shown in figure 6. Their unique construction involved a fixed length of Nichrome wire coiled within a glass tube and silver soldered at each end to a lug. A clear rubber hose was clamped over two tube holders forming a water tight jacket around the glass tube. Water flows through the tube to cool the wire inside. All metal parts were made from stainless steel.

These individually hand-crafted power resistors had a useful life of about 175 hours before failure. Failures were characterized by a gradual increase in resistance value as electrolytic corrosion of the nichrome wire at the water intake tee occurred. The sudden open circuit that resulted usually caused the system to lose control of model position. Clearly, a new design was needed to alleviate this problem.

A simple solution to this problem incorporates off-the-shelf water heater elements. As seen in figure 7, the new design includes a large aluminum tank with enough volume for all 36 of the necessary heater elements. The tank measures 30 in. O.D. and 28 in. high and has a volume of 39.5 cu ft. The resistor elements have an Incoloy sheath and range in overall length from 9 in. to 23 in. and in rated wattage from 2000 W to 6000 W. The elements are connected electrically in parallel and series combinations to achieve the desired resistances. A failure of one element can be detected by a discrete jump in total resistance. If necessary, an individual element can be easily replaced. The tank receives a continuous supply of low pressure water and includes safety interlocks. The success of this design is evident in the fact that no failures have occurred since the initial installation.

WIND TUNNEL TESTING

The first aerodynamic test conducted at Langley in the 6 inch MSBS was a store separation test. The objective of this test was to lower a suspended ogive cylinder model from a test section cavity into the freestream, allowing for cavity-model interactions to be studied.

A store separation demonstration was previously accomplished at the NASA Langley 13 inch MSBS. This facility uses optical position sensors to monitor the model position and does not allow for a wide range of vertical model positions as described in reference 3. Therefore, the suspended model remained stationary during the

demonstration while a plexiglas cavity structure, originally enclosing the model, was mechanically moved away to demonstrate store separation. Due to the unique capabilities of the 6 inch MSBS, the model can be lowered from a stationary cavity built into the test section. Optical model position detection would be very difficult with this configuration.

In preparation for the test, the test section was modified with an insert simulating the undercarriage of a fuselage. The insert, which consists of a leading edge, cavity, and trailing edge, is integrated into the existing test section. The leading edge of the insert was designed to smoothly deliver the incoming flow to the cavity. The cavity was designed specifically for an ogive cylinder test model.

The model, shown in figure 8, is one inch in diameter and five inches long. The cavity-model clearance is $1/2$ a model diameter front and rear, and $1/4$ diameter on each side. The trailing edge of the insert is a flat surface expanding the test section back to its original area. Figure 9 is a photograph of the test section with the insert.

System Calibrations

Prior to testing, several calibrations had to be completed on the system. These included a wind speed calibration; horizontal and vertical velocity profiles; drag, lift and lift position calibrations. These tests were necessary because of the physical changes in the tunnel and the fact that previous force calibrations had used a different model. Because of the reduced cross-sectional area of the tunnel, a new wind speed calibration was needed. A pitot-static tube was inserted into the center of the test section to measure the dynamic pressure. The dynamic pressure was then related to the pressure difference measured across the contraction.

During testing, the pitot-static tube is removed. However, the pressure difference across the contraction can still be monitored and the velocity obtained from the calibration. The velocity was also related to the fan speed, which can be used for a rough estimate of the wind speed. With the insert in the test section, the maximum velocity in the test section increased from Mach 0.5 to Mach 0.6. Figure 10 is a graph relating the dynamic pressure measured by the pitot-static tube and the pressure difference across the contraction.

After the wind speed calibration was completed, horizontal and vertical velocity profiles of the flow were recorded. These profiles were taken to verify that the flow was uniform across the test section. Figures 11 and 12 are horizontal and vertical profiles across the test section taken at Mach 0.5. Profiles at Mach 0.1 were also taken. Horizontally, the velocity is skewed so that there is about a three percent difference from one side to the other. There is approximately a two percent difference from the top to the bottom. Since most of the testing was done in a small area, these differences in the velocity across the test section were acceptable.

A drag calibration on the model was preformed next. The model was positioned just below the cavity, and a drag force was applied to it using weights and a pulley. A

feedback signal proportional to the drag current feedback signal was recorded as the weights were increased from 0 to 200 grams. This current feedback signal was monitored during testing to determine the drag forces on the model. The relationship between the current feedback signal and the drag was linear and a straight line fit of the data was sufficient. This data is presented in figure 13.

Two more drag calibrations were performed to investigate the relationship between drag and lift. The calibrations were carried out as before, except that a negative lift force was applied to the model during calibration. The lift force proved to have a negligible effect on the drag calibration, therefore simplifying the data reduction process.

The model was also calibrated in lift. Weights were applied to the model and the lift current feedback signal was recorded. A straight line was again fitted to the data which is presented in figure 14.

Finally, a lift position calibration was performed. The model was lowered out of the cavity and its position was monitored using a cathetometer. The cathetometer reading was correlated to the lift position signal which could be monitored during testing. The calibrations allow drag and lift forces on the model to be monitored during testing and related to the position of the model relative to the cavity.

Flow Visualization

The flow visualization system used for the store separation test consisted of two basic components. A fog generator was placed in front of the contraction to inject vaporized propylene glycol into the flow. At the test section, two 5 mW lasers and beam spreading optics were used to illuminate the flow above and below the model. The optics spread the beams into light sheets which could be positioned either perpendicular or parallel to the model. A video system including a CCD camera was used for live viewing and recording of the flow around the model.

The first series of flow visualization tests involved lowering the model from the cavity into a set of smoke streams. Figure 15 is a photo of the model suspended just below the cavity. Before experimenting with the light sheets, the test section was brightly illuminated to observe the position of the smoke streams. Figure 16 shows smoke contouring to the bottom of the model at $M=0.15$. For test runs with the light sheet, smoke streams were positioned approximately 1/2 inch from the cavity at approximately 1/4 inch spacing. The smoke streams were then observed using two longitudinal light sheets to illuminate above and below the model along its axis of symmetry.

As the model enters the oncoming flow, the smoke streams are shown to contour to the model followed by the entrainment of smoke into the boundary layer. Further lowering of the model reveals the uppermost smoke stream contouring to the top of the model. This stream is very compact along the model nose, however, as the stream reaches the forebody, it begins to expand greatly. This pattern does not occur below the model. Figure 17 illustrates this phenomena. This is believed due to separation occurring

over the upper surface (leeward side). Separation may result from the upward bending of streamlines in the vicinity of the model nose and the cavity leading edge as the flow adjusts itself to the cavity. Therefore, the model may experience an effective angle of attack with an associated cross-flow resulting in separation on the leeward side.

It was decided that further flow visualization tests were necessary to study the model-cavity interaction. A second series of flow visualization tests was attempted using a cross sheet to view the flow between the cavity and the model. The viewing area allowed access of the model nose and most of the forebody. Upon lowering the model approximately 1/4 of a diameter out of the cavity, the cross sheet revealed an undistinguishable smoke pattern between the cavity on the model that reached into the cavity. It is believed that no distinguishable patterns are revealed in this region due to the extremely high turbulence levels present in cavity flow.

However, upon further lowering the model, a distinct lightning-shaped pattern emerges from the undistinguishable pattern extending to the model. This pattern wraps around the model revealing the entrainment of smoke in the boundary layer. These patterns occur along the model nose, but the lightning-shaped pattern tends to break up along the forebody. It is not presently known what the lightning-shaped pattern represents. Figure 18 illustrates cross sheets at two locations on the model nose. Further flow measurements using, for example, Laser Doppler Velocimetry are necessary to detail this phenomena.

Store Separation Tests

The initial store separation tests occurred at fixed Mach numbers between 0.1 and 0.3. Drag forces acting on the model were extracted through a calibration of the drag current feedback signal previously discussed. Results for a Mach number of 0.25 are presented in figure 19. The turbulent nature of cavity flow is quite evident from the scatter present while the model is in the cavity. The scatter is shown to decrease as the model begins its move out of the cavity. Furthermore, the drag coefficient increases as the model begins to lower. This increase is evident until the model is completely clear of the cavity. Further lowering of the model has no effect on the drag coefficient, signaling the model is free of any cavity interactions and is completely emerged in the freestream.

Upon completion of the store separation tests at fixed Mach numbers, a series of tests was conducted with the model suspended just inside the cavity so that simultaneous lift and drag measurements could be made with increasing Mach numbers. The Mach number range for this series of tests was 0.1 - 0.5. Lift and drag coefficient data are presented in figure 20. As discussed previously, measurements do fluctuate significantly about a mean, especially at the higher Mach numbers due to the turbulent nature of cavity flow. Therefore, lift and drag values presented in figure 20 represent mean values of data taken over 30 second intervals at 1 Hz.

Results indicate a significant decrease in the drag coefficient from 0.37 to 0.15 with a Mach number increase from 0.1 to 0.3, respectively. For Mach numbers greater than

0.3, the drag coefficient remains nearly constant ($0.15 > C_d > 0.13$), therefore showing little dependence with Mach number in this range. It is interesting to note that for Mach numbers greater than 0.3 the drag coefficient of the model in the cavity is significantly lower than that measured in the freestream. Figure 19 shows that the drag coefficient of the model in the freestream is approximately 0.35.

Lift coefficient results show that for the entire Mach number test range, a small negative lift acts on the model. This was observed during testing as the model position would tend to lower with increasing Mach number as if the model was being "pushed" out of the cavity. Due to this effect, it was necessary to monitor the EPS signal so that adjustments could be made to bring the model back to its original position. A general overview of the lift coefficient data shows that trends are not as nearly pronounced as for its drag counterpart; however, some trends are established. For instance, an initial increase occurs in the lift coefficient from -0.11 to -0.06 with increasing Mach numbers between 0.1 and 0.15. After this initial trend, increasing the Mach number has little effect except for a slight decrease in the lift coefficient.

These tests were repeated using a 1/2 scaled version of the original store model. Trends in lift and drag data with varying Mach number are similar between the scaled models; however, a significant spin developed on the smaller model not observed in the original tests. The spin was counter-clockwise (front view) and signified a rolling moment produced by the cavity-model interaction. A spinning motion was not observed with the model in the freestream. The spin occurred at Mach 0.2 and was preceded by a pronounced rocking motion at lower Mach numbers. Present with this spinning motion were pronounced oscillations in pitch starting at $M=0.1$. As described earlier, these oscillations were only observed on the larger model at $M=0.3$ as the model separated from the cavity.

CONCLUSION

The initiative to make the 6 Inch MSBS fully operational was successful. The photographs of figure 21 show three views of a space shuttle model in suspension. The system's angle of attack capabilities are evident. Although roll control is not presently operational, roll stiffness using cambered model cores has been demonstrated.

Implementation of the new EPS electronics has significantly improved system performance through reduced noise and drift. System reliability was greatly improved with the addition of a new water cooled resistor system as well as rewiring the compensation system interconnections.

Simulation of cavity store separation was successfully demonstrated. Moreover, it is unlikely that the tests performed in the 6 Inch MSBS could be duplicated in other facilities. The system performed flawlessly during the tests.

The power supply system of the 6 Inch MSBS remains the primary weakness. A 1970 MIT proposal to Langley for continued studies of the system requests funding for a

complete power supply upgrade. Only a small portion of the proposal was ever implemented. Optimum performance will not be achieved without a ten-fold increase in power capability. Bi-polar, solid state power supplies would increase model stiffness and system frequency response.

Future enhancements to the system would include the replacement of existing power supplies and compensation system electronics. A minicomputer has been purchased for implementation of digital control of model position in five degrees of freedom. The system has not been fully calibrated while at Langley; therefore, a full five degree of freedom force calibration is planned. A special balance fixture designed specifically for suspension in the 6 inch MSBS has been fabricated.

ACKNOWLEDGEMENTS

The authors would like to express their gratitude to Dr. Colin Britcher of Old Dominion University for his technical guidance and support. Further appreciation goes to the Pressure and Flow Measurement Section and Photo-Optical Instrumentation Section for their assistance.

REFERENCES

1. Stephens, Timothy: Design, Construction, and Evaluation of a Magnetic Suspension and Balance System for Wind Tunnels. NASA CR-66903, 1969.
2. Daniels, Taumi S. and Tripp, John S.: Improvements to an Electromagnetic Position Sensor for a Magnetic Suspension Wind Tunnel. International Instrumentation Symposium (Albuquerque, New Mexico), May 1988, pp. 65-70.
3. Tchong, P. and Schott, T. D.: A Five Component Electro-Optical Positioning System. 12th International Conference on Instrumentation in Aerospace Simulation Facilities (Williamsburg, Virginia.), June 1987, pp.322-333.

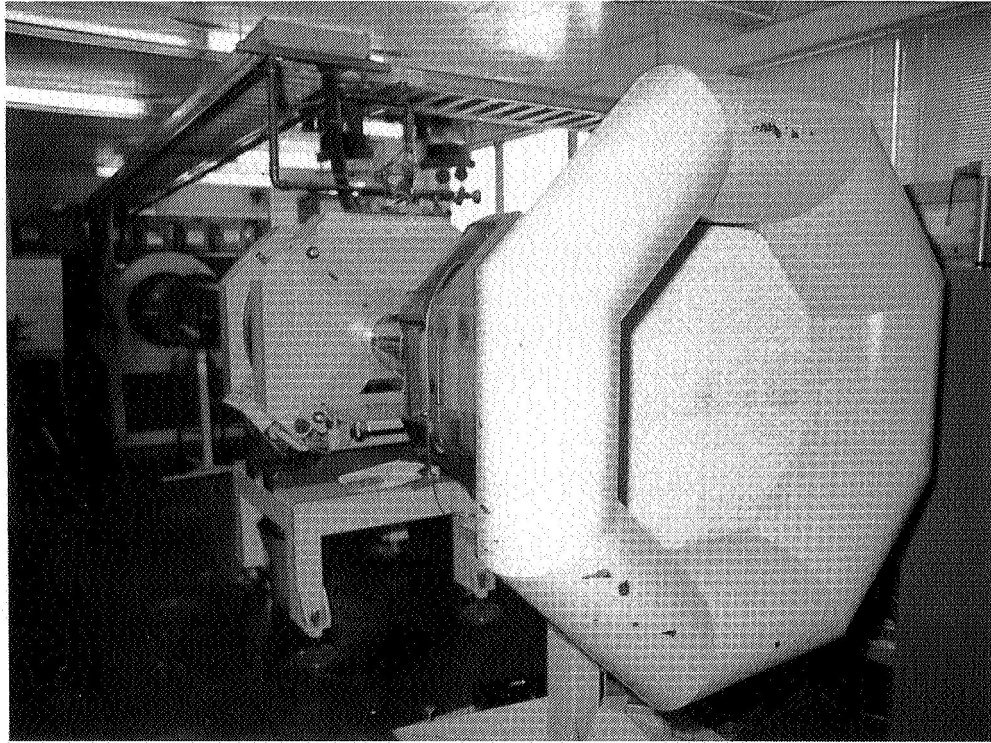


Figure 1. Downstream view of 6 inch MSBS.

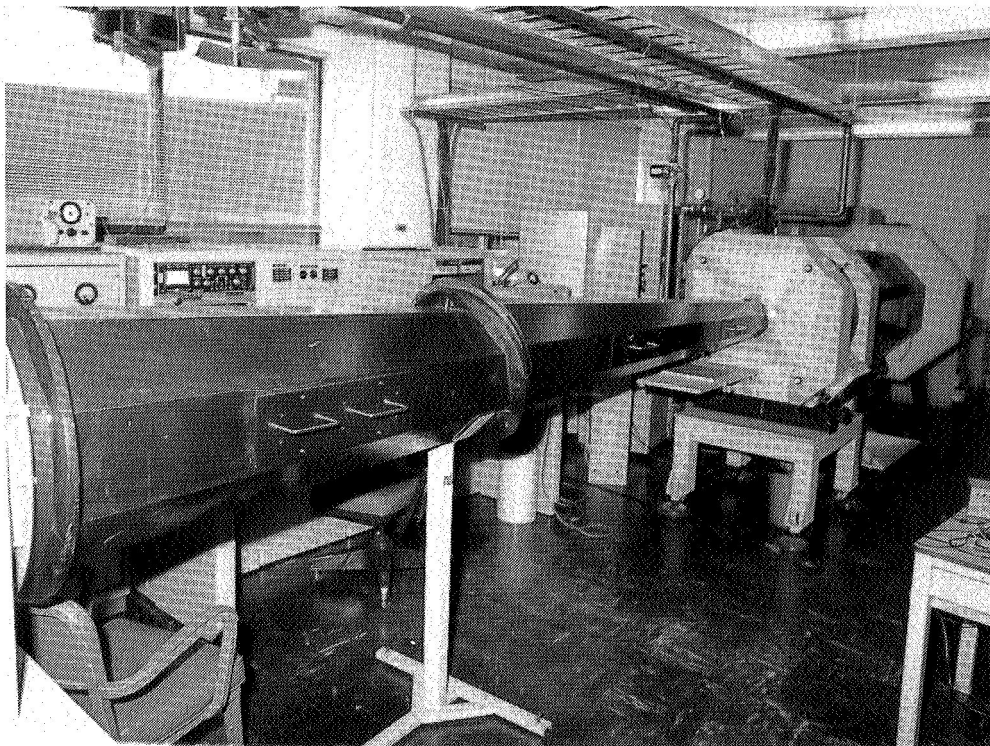


Figure 2. Upstream view of 6 inch MSBS.

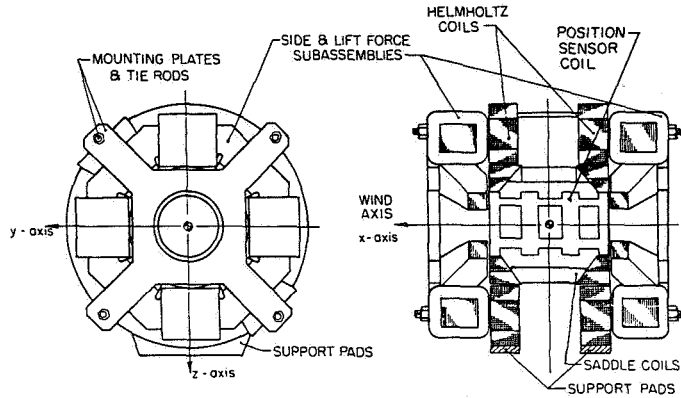
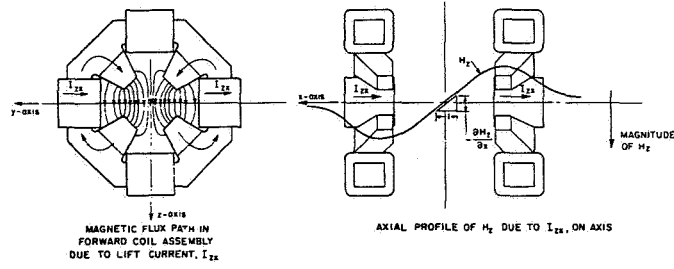


Figure 3. End and sectional views of magnet configuration.

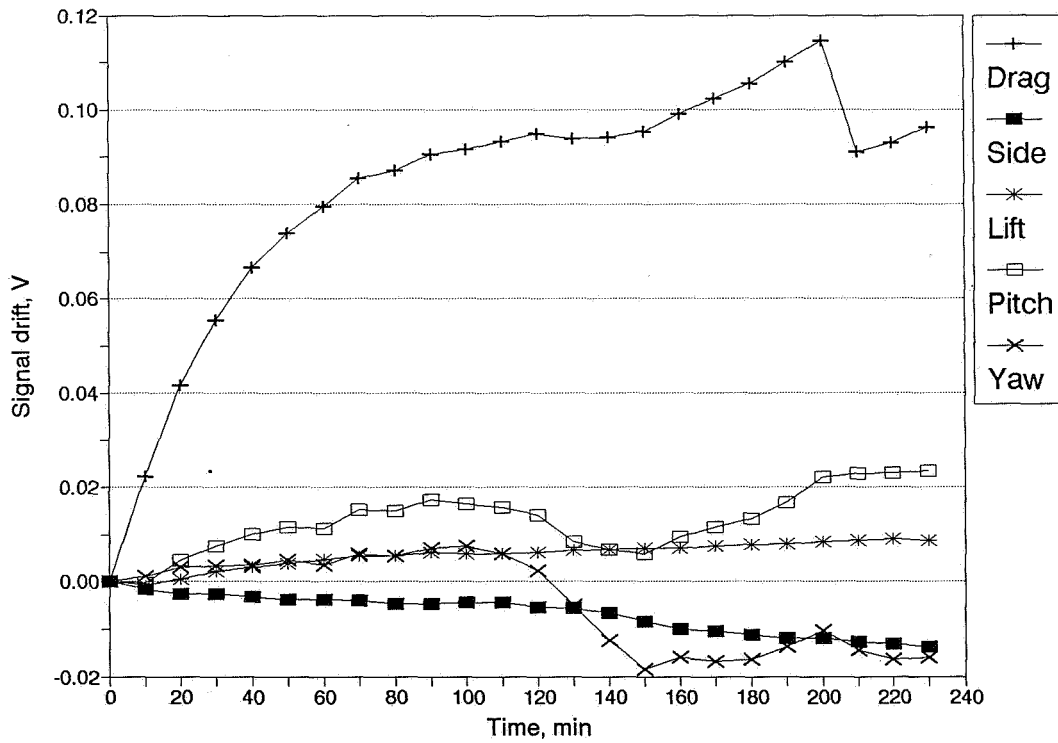


Figure 4. EPS position signal drift.

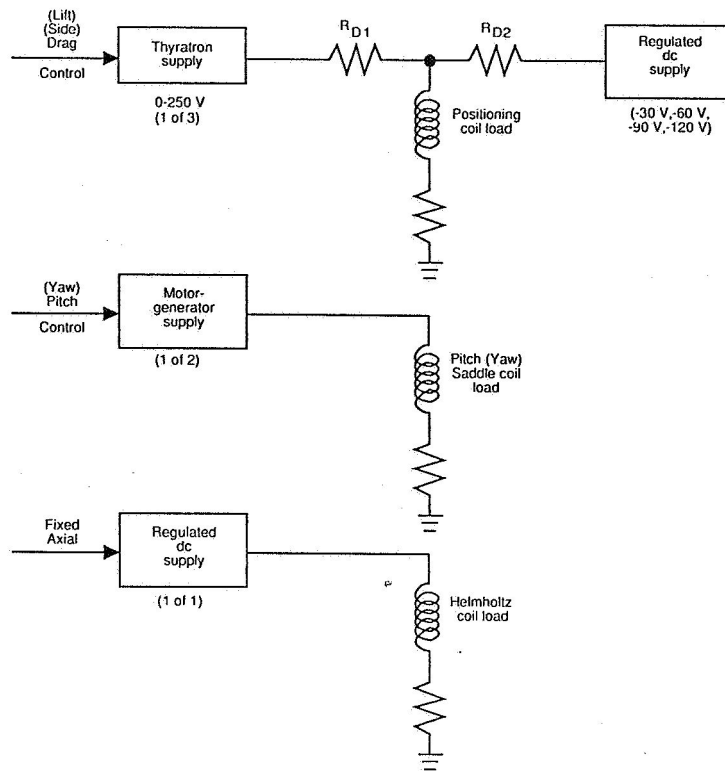


Figure 5. Power supply system schematic.
 ORIGINAL PAGE
 BLACK AND WHITE PHOTOGRAPH

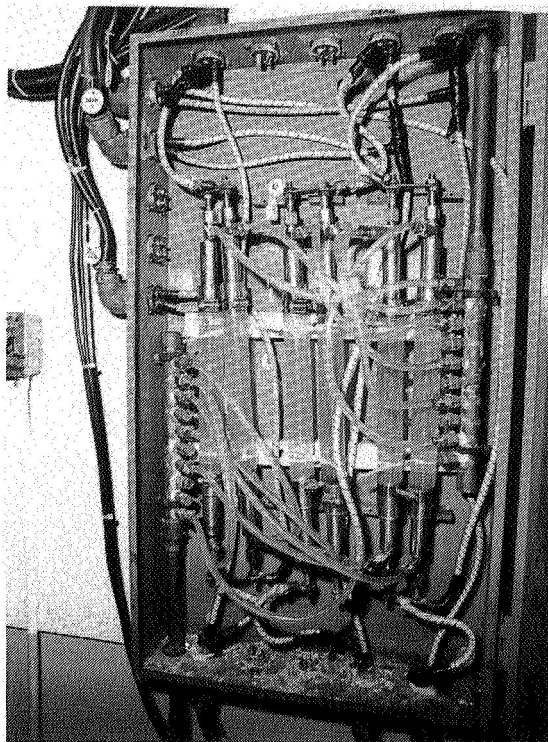


Figure 6. Original water cooled resistors.

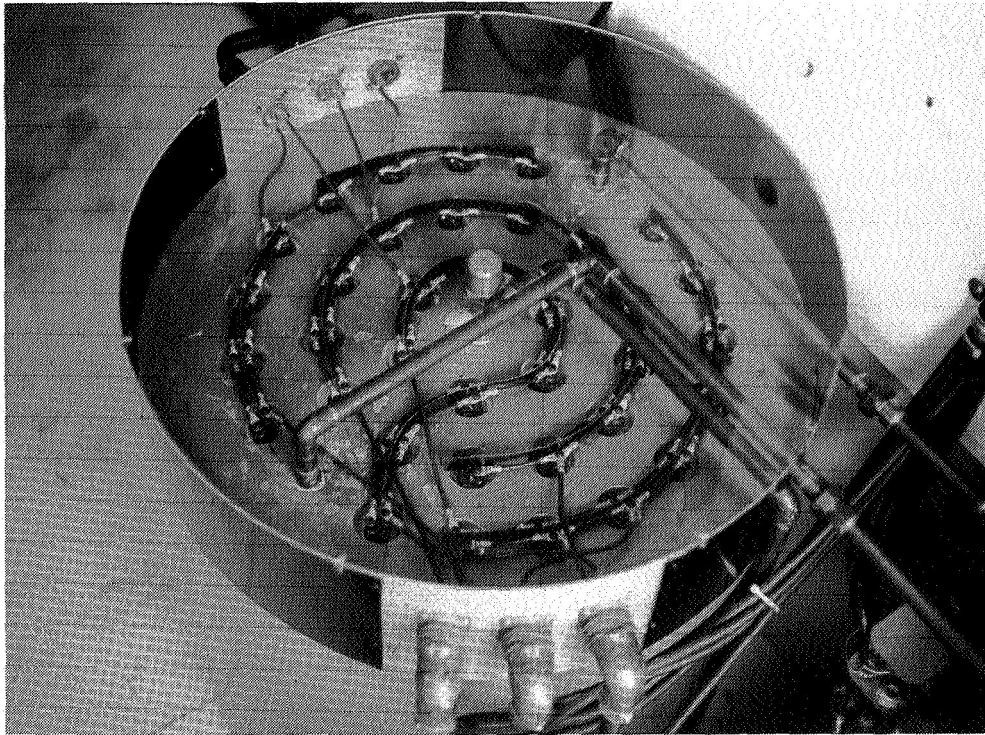


Figure 7. New power resistor system.

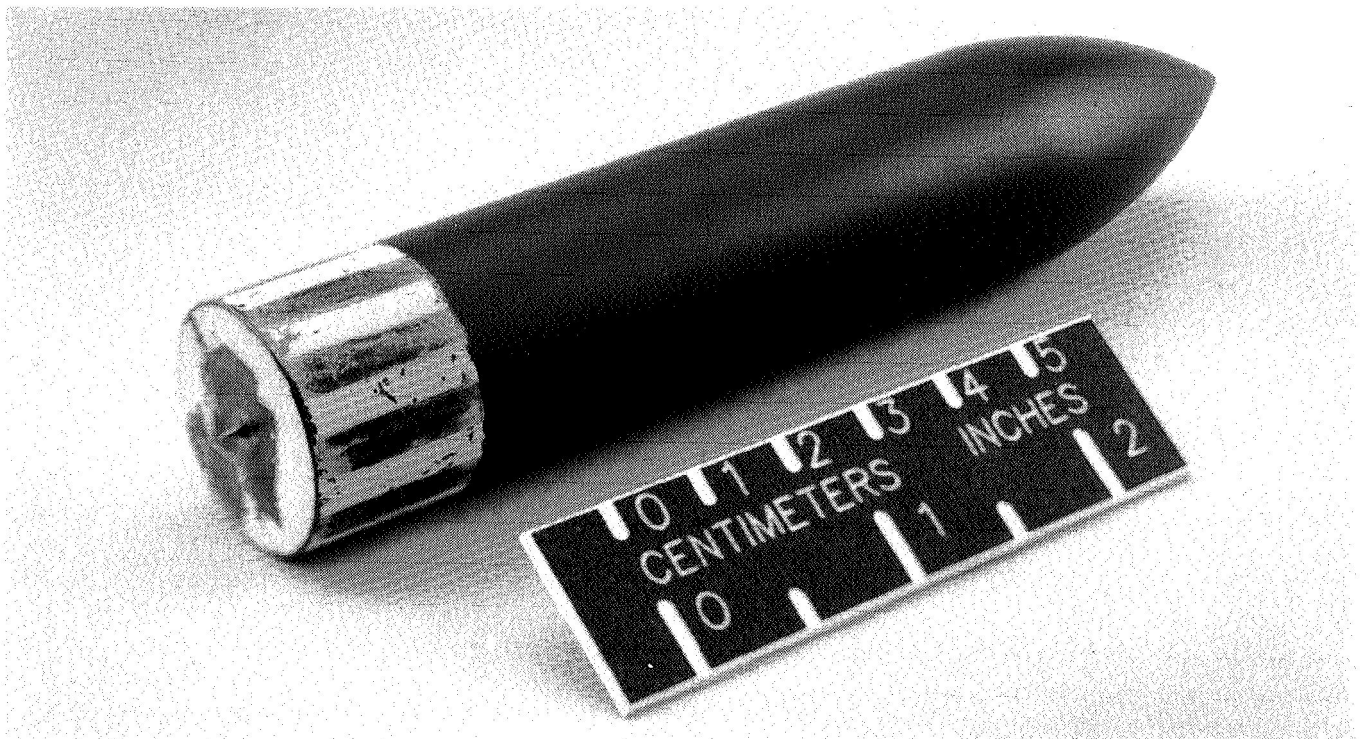


Figure 8. Store separation model.

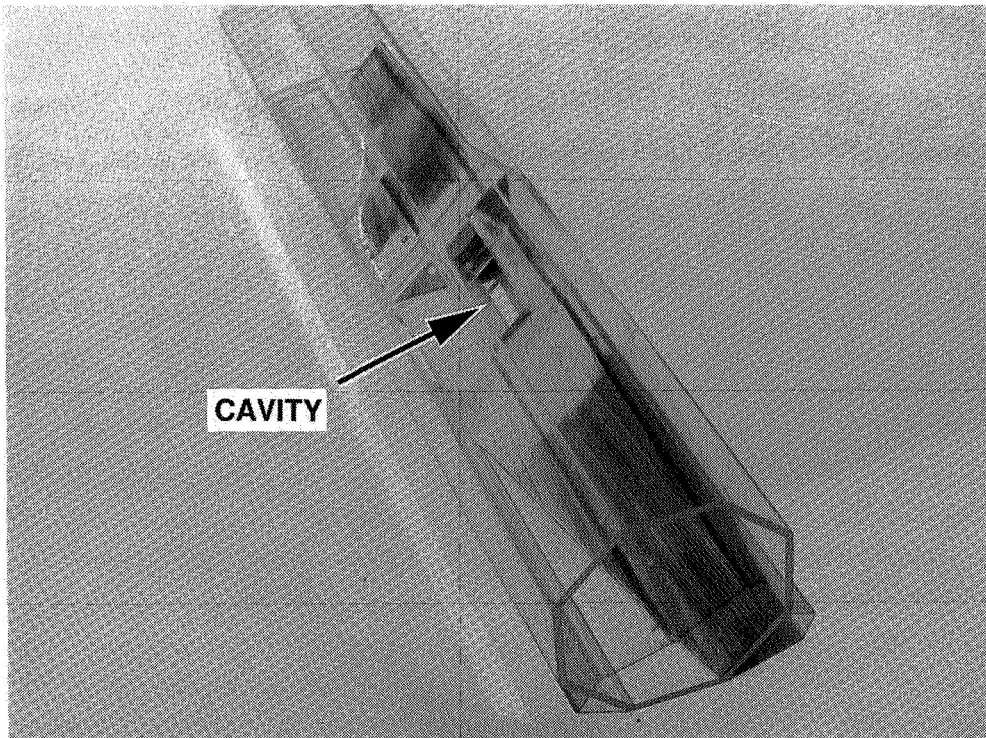


Figure 9. Test section with cavity insert.

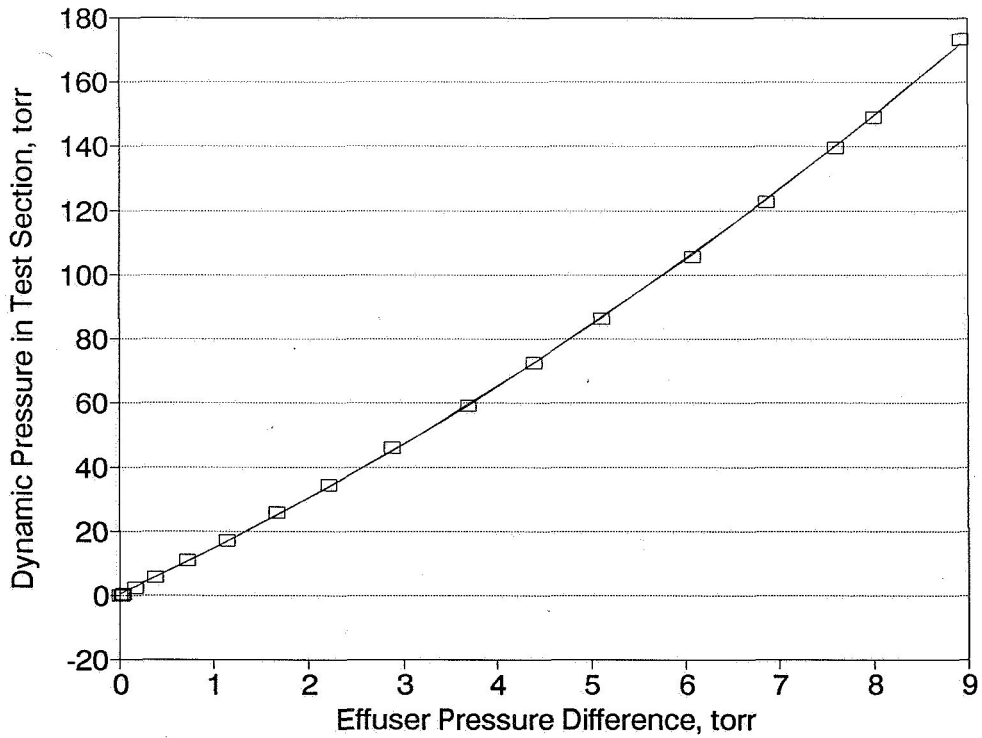


Figure 10. Test section calibration.

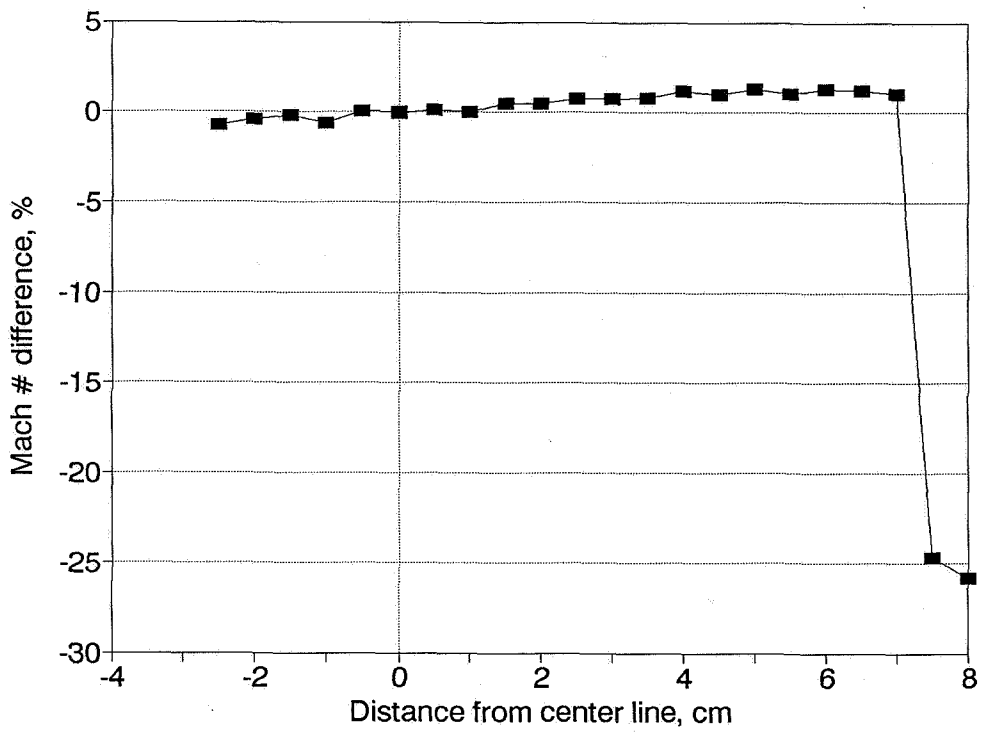


Figure 11. Horizontal velocity profile ($M=0.5$).

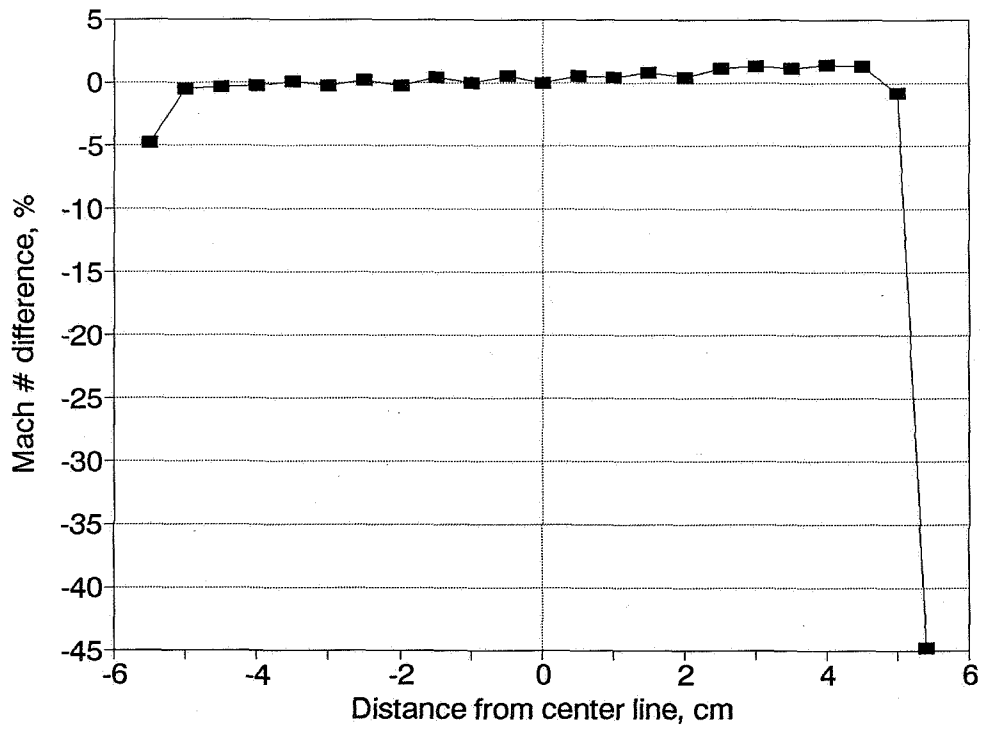


Figure 12. Vertical velocity profile ($M=0.5$).

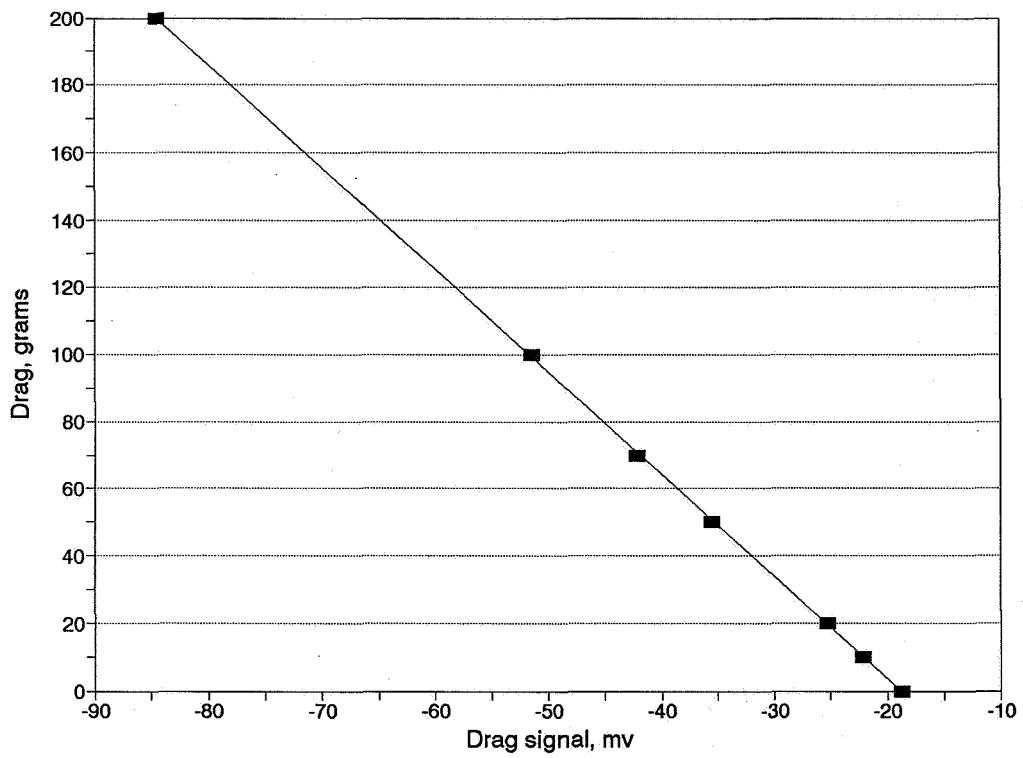


Figure 13. Drag calibration of store separation model.

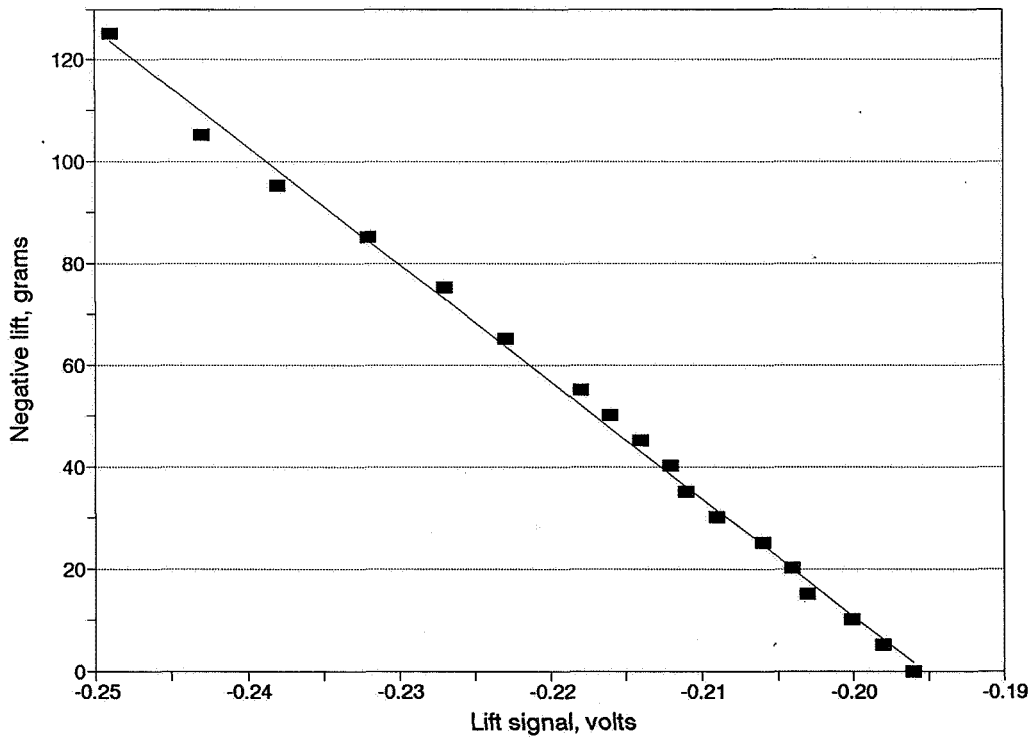


Figure 14. Lift calibration of store separation model.

ORIGINAL PAGE
BLACK AND WHITE PHOTOGRAPH

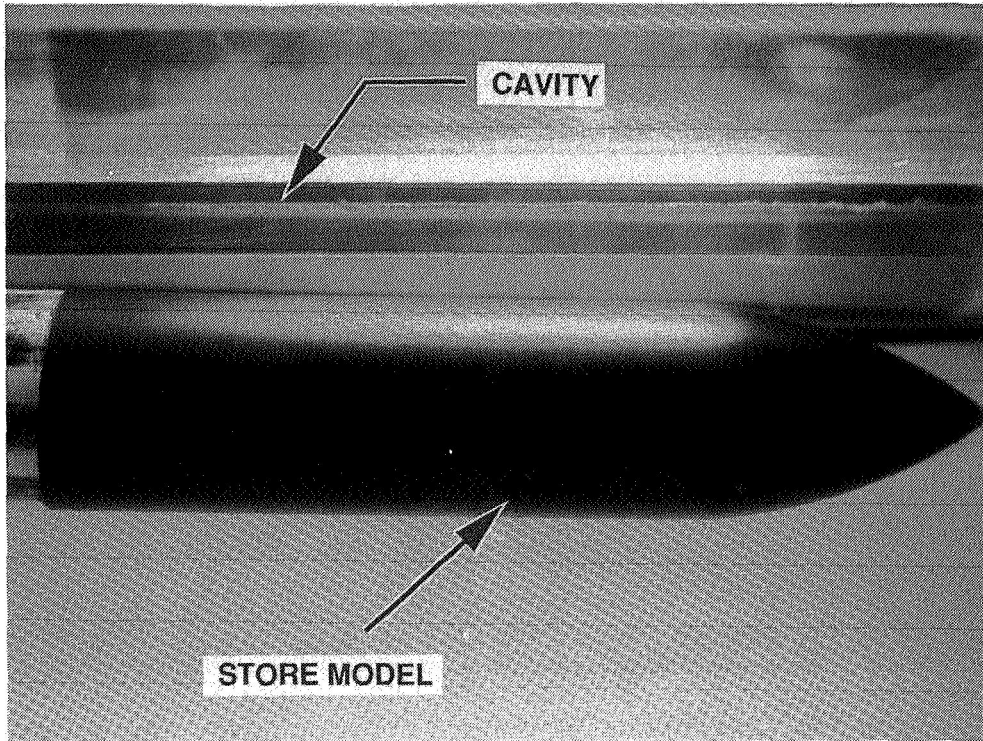


Figure 15. Suspended model below cavity.

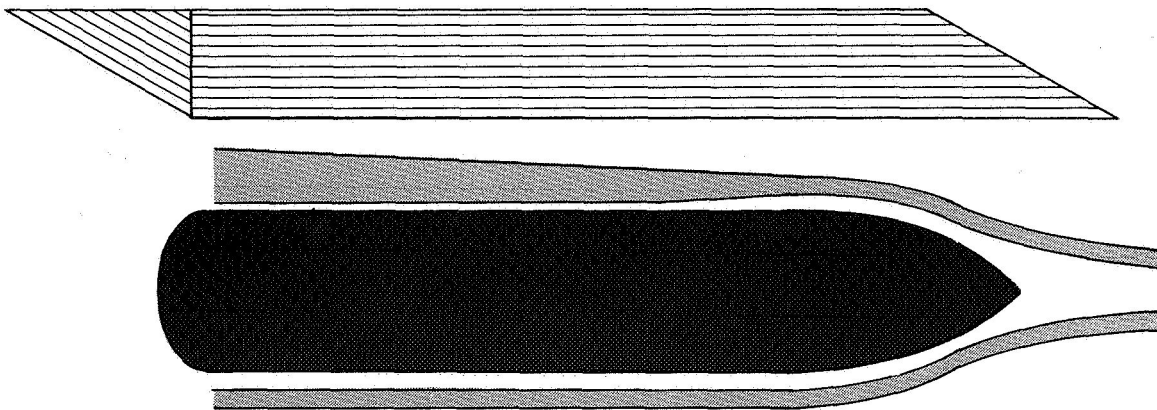


Figure 16. Smoke contouring to model.

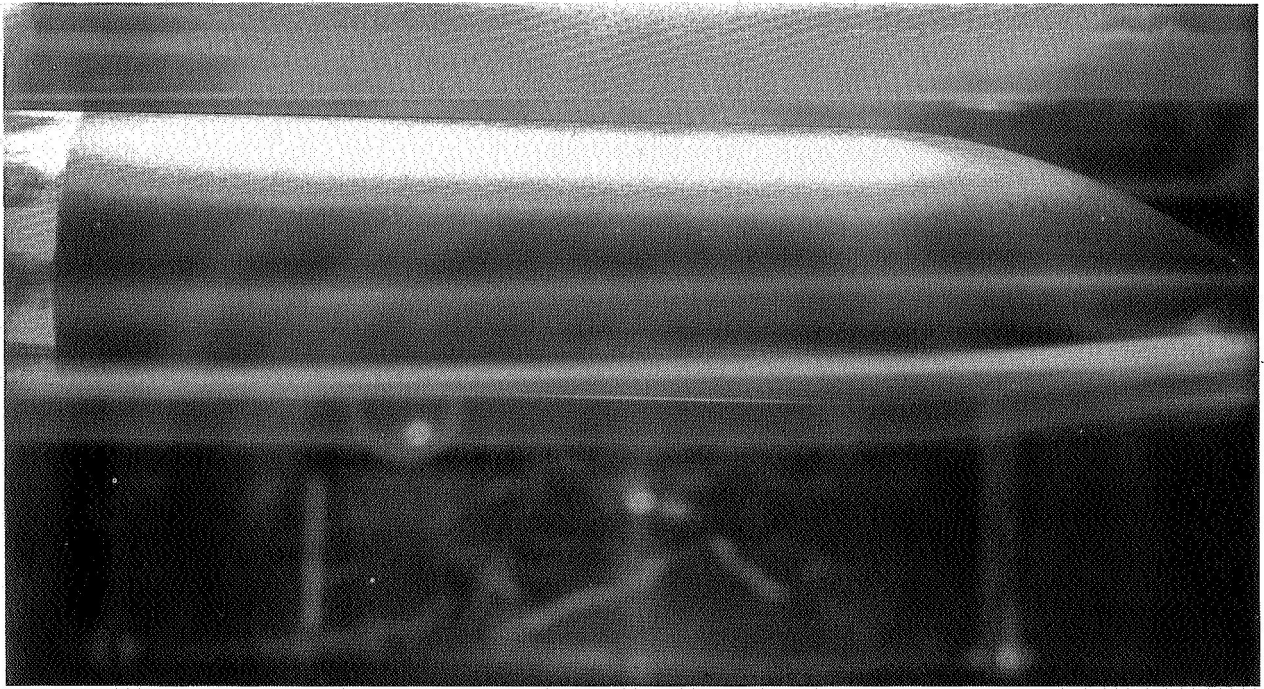


Figure 17. Longitudinal light sheet showing cavity interaction ($M=0.15$).

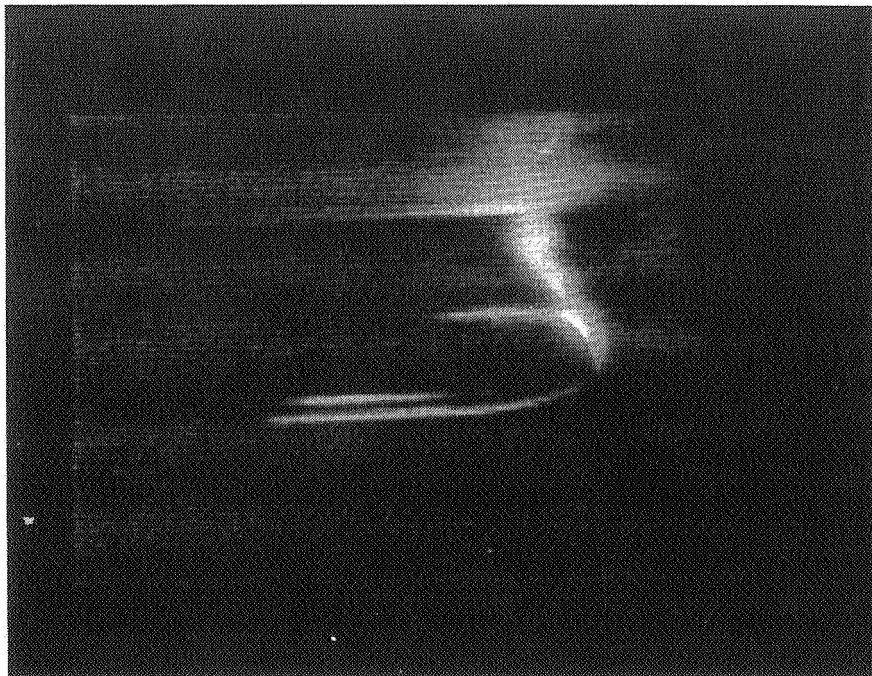


Figure 18. Cross light sheet showing cavity interaction ($M=0.15$).

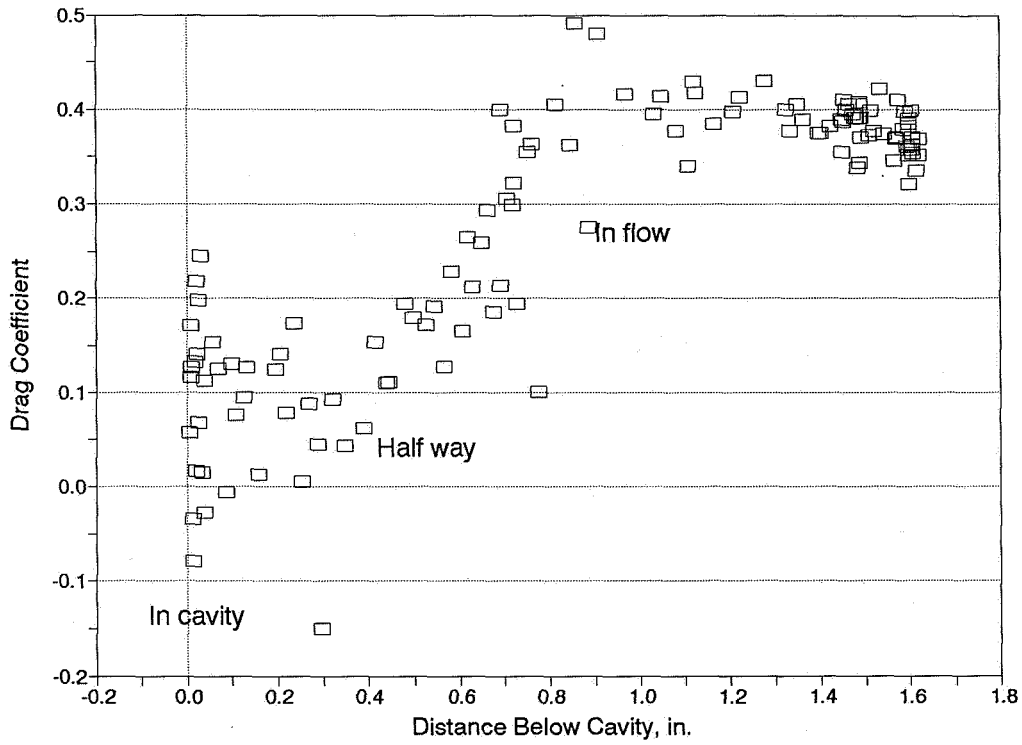


Figure 19. Effect of model position on drag coefficient.

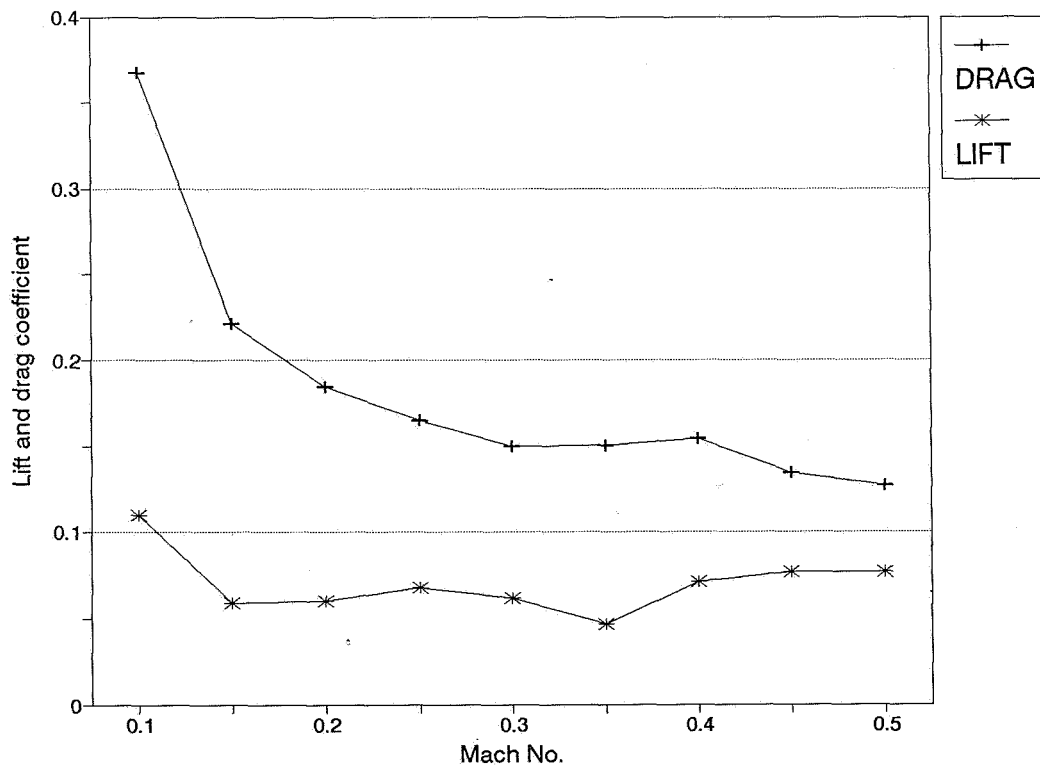


Figure 20. Effect of Mach number on lift and drag coefficient.

ORIGINAL PAGE
BLACK AND WHITE PHOTOGRAPH

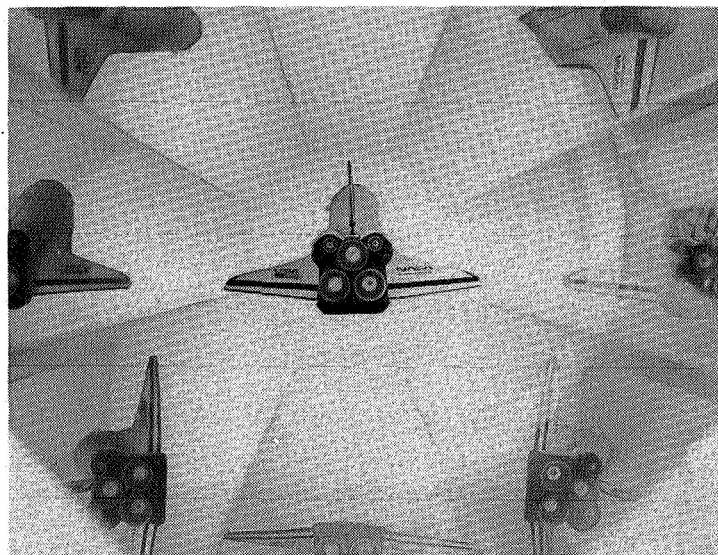
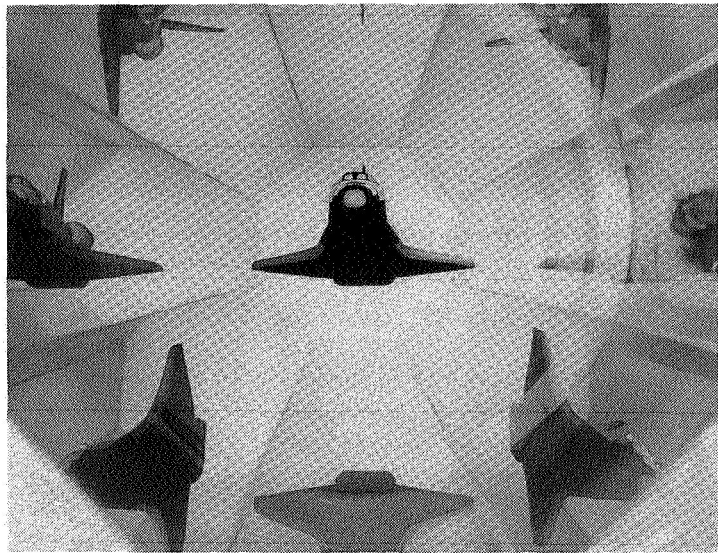
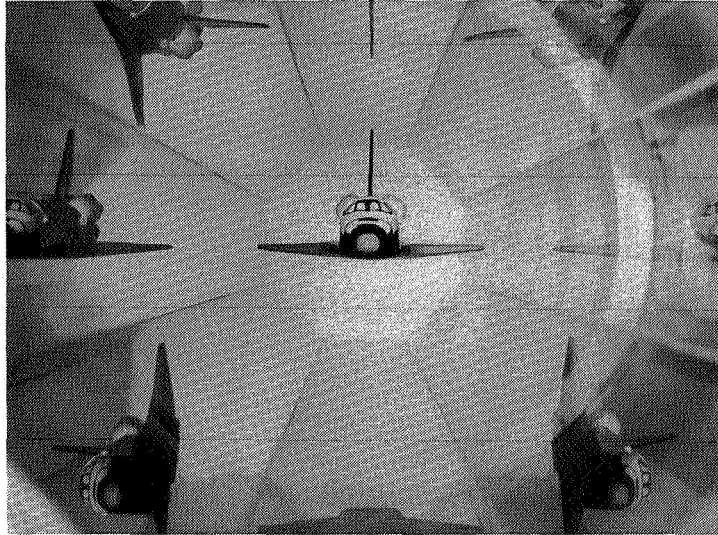


Figure 21. Three photographs of space shuttle model.